Gated Mesoporous Silica Nanoparticles Using a Double-Role Circular Peptide for the Controlled and Target-Preferential Release of Doxorubicin in CXCR4-Expresing Lymphoma Cells

Cristina de la Torre, Isolda Casanova, Gerardo Acosta, Carmen Coll, María José Moreno, Fernando Albericio, Elena Aznar, Ramón Mangues, Miriam Royo,* Félix Sancenón, and Ramón Martínez-Máñez**

B-cell non-Hodgkin's lymphoma (B-NHL) is the most frequent malignant lymphoid neoplasm, which has a high degree of relapse and chemoresistance. Thus, strategies to improve currently used therapies are needed. In this context, a new CXCR4-targeted delivery system is described using mesoporous silica nanoparticles (MSNs) that are loaded with doxorubicin and capped with a derivative of the T22 peptide (P). This design makes full use of the great affinity of the T22 peptide to CXCR4 receptor, which is overexpressed in lymphoma cells. The peptide is able to guide the gated nanoparticle to B-NHL cells to facilitate MSNs uptake via the CXCR4 receptor. The endocyted P-capped MSNs are also opened by endosomal proteolytic enzymes to allow intracellular doxorubicin delivery.

1. Introduction

In the last few years, nanotechnology has proved an innovative approach for drug-delivery therapies. The development of drug-release systems capable of delivering active molecules to certain cells in a controlled manner is a timely pursued goal. In this scenario, mesoporous silica nanoparticles (MSNs) have been demonstrated to be excellent reservoirs and vehicles for drug storage[1–5] because of their unique mesoporous structure, large specific volume, and easy functionalization. MSNs are also considered biocompatible, can be uptaken by cells via endocytosis, and can be functionalized with a large collection of switchable molecular/supramolecular pore-capping ensembles to develop gated MSNs capable of retaining a cargo and delivering it upon the application of a specific chemical[6–12] (e.g., redox molecules, selected anions, and pH changes), physical[13–18] (e.g., light, temperature, or magnetic fields) or biochemical (e.g., enzymes, antibodies, or DNA) stimuli.[19–24] Furthermore, thanks to the easy surface functionalization in MSNs, the possibility of decorating them with additional functional elements as targeting ligands opens up new possibilities in the design of gated delivery nanodevices.[25]

In this context, the use of biomolecules in capped mesoporous nanostructures has proved useful in the design of delivery systems for applications in more biological and realistic settings. Among

C. de la Torre, Dr. C. Coll, Dr. E. Aznar,
Dr. F. Sancenón, Prof. R. Martínez-Máñez
Centro de Reconocimiento Molecular y
Desarrollo Tecnológico (IDM)
Unidad Mixta Universitat Politècnica de València-Universitat
de València and CIBER de Bioingeniería
Biomateriales y Nanomedicina (CIBER-BBN)
Camino de Vera s/n
46022 Valencia, Spain
E-mail: rmaez@qim.upv.es

Dr. I. Casanova, Dr. M. J. Moreno, Prof. R. Mangues
Grup d'Oncogènesi i Antitumorals
Institut d'Investigacions Biomèdiques Sant Pau
Hospital de Sant Pau and CIBER de Bioingeniería
Biomateriales y Nanomedicina
Sant Antoni Maria Claret 167
Pavelló 11, 08025 Barcelona, Spain
E-mail: rmangues@santpau.cat

DOI: 10.1002/adfm.201403822

G. Acosta, Prof. F. Albericio
Institute for Research in Biomedicine
Barcelona Science Park-University of Barcelona
and CIBER de Bioingeniería
Biomateriales y Nanomedicina (CIBER-BBN), Baldiri Reixac 10
08028 Barcelona, Spain

Prof. F. Albericio
Department of Organic Chemistry
Universitat de Barcelona
08028 Barcelona, Spain

Prof. F. Albericio
School of Chemistry Yachay Tech
Yachay City of Knowledge
Urcuqui, Ecuador

Dr. M. Royo
Combinatorial Chemistry Unit
Barcelona Science Park and CIBER de Bioingeniería
Biomateriales y Nanomedicina (CIBER-BBN), Baldiri Reixac 10
08028 Barcelona, Spain
E-mail: mroyo@pcb.ub.es

biomolecules, the employment of peptides is especially appealing since their use in combination with MSNs is envisioned to offer great potential, and may provide exquisite selectivity in the design of advanced gate-opening devices for highly specific applications. In recent years, scientists have developed different exploratory works on the design of peptide-capped nanoparticles capable of being hydrolyzed by proteases.[26–31] However, many of these studies have focused on the mode of anchoring peptidic chains or in conformational changes to trigger the gating mechanism. In parallel, researchers have also explored the targeting functionality of short peptides to help gated nanoparticles reach their cellular target with satisfactory results.[32–37] However, the use of peptides for a double role (e.g., targeting and gating) is scarce in MSNs.[38]

In this work, we paid attention to B-cell nonHodgkin's lymphoma (B-NHL), the most frequent malignant lymphoid neoplasm. Its standard treatment combines chemotherapy (e.g., cyclophosphamide, doxorubicin, vincristine, and prednisolone) with Rituximab, a monoclonal antibody that targets CD20.[39,40] Despite most B-NHL patients initially respond to chemotherapy, with about 40%–50% complete responses, many of them undergo relapse.[41]

Drug resistance in relapsed lymphomas is partly acquired by homing lymphoma cells to bone marrow microenvironment, where interaction with stromal cells stimulates their survival and confers chemoresistance.[42] This interaction is mainly regulated by chemokine receptor CXCR4, which is expressed in the membrane of lymphoma cells and is activated by the chemokine CXCL12. The CXCR4/CXCL12 axis is involved in the survival and trafficking of malignant B cells, and in their homing to lymph nodes.[43] CXCR4 overexpression has also been associated with poor prognosis in several B-cell malignancies.[44,45] Moreover, in diffuse large B-cell lymphoma, the most frequent B-NHL subtype, CXCR4 expression enhances cell dissemination and associates with shorter patient survival.[46] In this context, targeting chemotherapeutic agents to CXCR4-overexpressing, lymphoma cells may be important to overcome chemoresistance. A suitable approach to achieve this goal would be to develop delivery carriers that are able to selectively reach the CXCR4 receptor. However, as far as we know, such targeted release systems have not yet been described.

With this background, and taking into account the need to develop new delivery carriers to overcome usual side effects and chemoresistance in lymphoma, we were interested in attempting the design of a targeted delivery system to B-NHL cells. The controlled-release nanomaterial we prepared is shown in **Scheme 1**. It consists of mesoporous nanoparticles that were loaded with the cytotoxic drug doxorubicin. As the capping and targeting agent, we also selected an engineered version polyphemusin II peptide from the horseshoe crab named T22. In the engineered peptide, three substitutions at residues Tyr5, Lys7, and Tyr12 dramatically enhanced the affinity of natural peptide T22 for the CXCR4 receptor.[47–49]

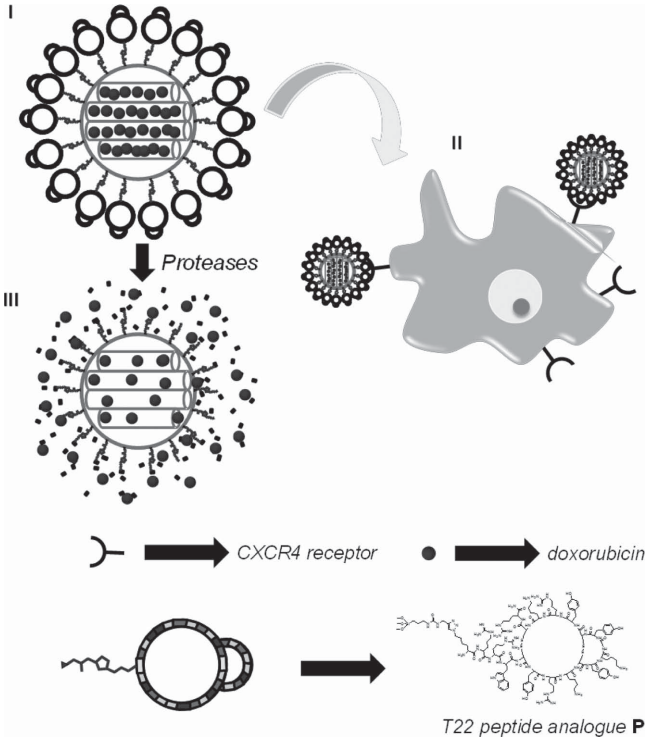

Scheme 1. Representation of the targeted- and capped-proposed system. I) Solid **S2** is capped with targeting T22 peptide analogue **P**, which inhibits the release of entrapped doxorubicin. II) The targeting gated system is recognized by the CXCR4 receptor and is endocyted. III) Doxorubicin delivery from **S2** is triggered by proteases.

2. Results and Discussion

2.1. Design and Synthesis of Peptide-Gated MSN

In the present work, MCM-41-based MSNs were selected as an inorganic scaffold. The nanoparticulated mesoporous support was prepared by using tetraethyl orthosilicate (TEOS) as a hydrolytic inorganic precursor and surfactant hexadecyltrimethylammonium bromide (CTABr) as the porogen species. After surfactant removal by calcination, bare MSNs were obtained. The inorganic support was then loaded with antitumoral drug doxorubicin, and the outer surface of the nanoparticles was functionalized with propargyl-containing linker 1-(3-(triethoxysilyl)propyl)-3-prop-2-ynyl-urea (**1**) (see the Experimental Section for details), obtained by the nucleophilic addition of propargylamine to 3-(triethoxysilyl)propylisocyanate. This procedure yielded solid **S1**.

An azide-containing analogue of peptide T22 with Lys(N_3) in the N-Terminal (**P**) was obtained by Fmoc solid-phase synthesis using a Rink amide ChemMatrix resin and all the Cys side chains protected with the Trt group. Having finished peptide elongation, the peptide was cleaved from the resin using the TFA–TIS-H_2O mixture at 25 °C for 1 h. This linear peptide was then oxidized for its cyclization using dimethyl sulfoxide (DMSO) as an oxidizing agent and was purified by semipreparative high-performance liquid chromatography (HPLC) with a mass spectrometry detector (HPLC-MS) to obtain the final azide-T22 derivative (**P**), which is depicted in **Scheme 2**. The product was characterized by high resolution mass spectrometry (HRMS) (calcd. for $C_{115}H_{178}N_{42}O_{23}S_4$ $[M^{+4}H]^{4+}$ 660.8227, found 660.8236) and a peptide content of 86% was obtained. The peptide was also studied by circular dichroism and the spectrum exhibited a strong negative band at 210 nm and a

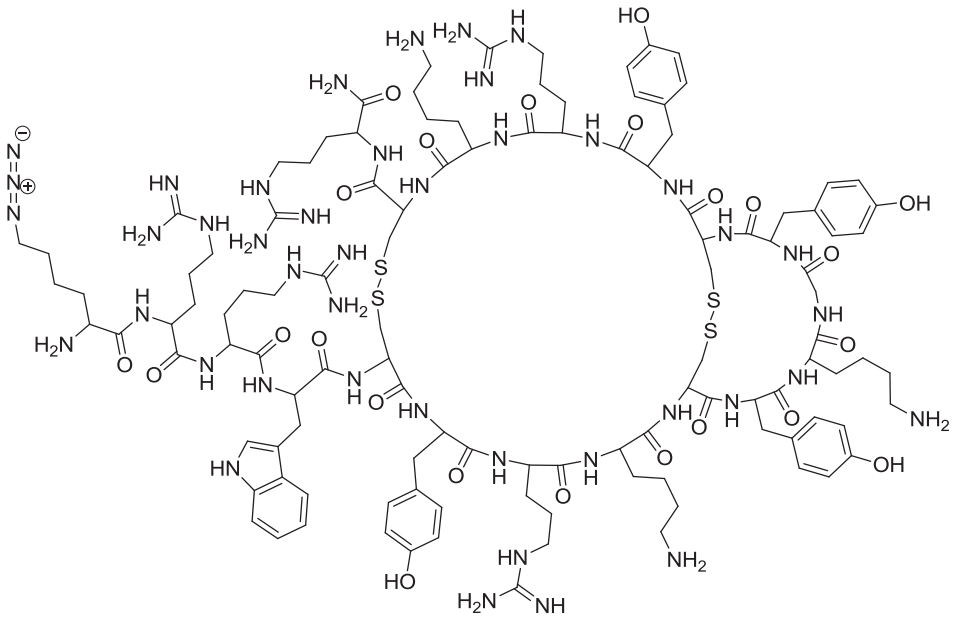

Scheme 2. Structure of the final azide-containing T22 analogue peptide (**P**).

strong positive band near 200.6 nm, and was similar to that described for T22[50] (see Figure SI-3, Supporting Information).

Finally, the capped nanoparticles **S2** were prepared using a "click" reaction between **S1** and the azide-containing T22 analogue peptide **P**. The peptide was expected to form a dense targeting layer around the MSNs capable of retaining doxorubicin inside pores. Doxorubicin delivery was also expected to occur in the presence of proteases that were able to hydrolyze the amide bonds in the peptide.

2.2. Materials Characterization

Once obtained, all the prepared solids were characterized by standard procedures for hybrid organic–inorganic mesoporous materials. First, the ordered structure of the inorganic supports was carefully studied. The typical MCM-41 structure of the starting material was confirmed by powder X-ray diffraction (PXRD) both before and after the calcination step to obtain an empty ordered framework of mesopores (see **Figure 1**a,b). As seen in Figure 1, the PXRD pattern of the as-synthesized siliceous nanoparticulated MCM-41 shows the typical low-angle reflections of a hexagonal array. After the calcination step, a significant displacement of the main peak (assigned to the (100) Brag reflection) was observed, which corresponded to an approximate cell contraction of 4 Å. This displacement and the broadening of the (110) and (200) peaks were related to the further condensation of the silanol groups in the calcination step. The PXRD pattern of solid **S1** was also recorded (Figure 1c). In this case, a slight intensity decrease of the (100) reflection and a broadening of the (110) and (200) reflections were observed, most likely due to loss of contrast in relation to the pore voids filling with doxorubicin. Nevertheless, the value and intensity of the (100) peak in this pattern strongly evidenced that the loading process with the dye and the further functionalization did not damage the mesoporous 3D MCM-41 scaffolding.

The morphology in solids **S1** and **S2** was also studied by transmission electron microscopy (TEM) (**Figure 2**). In the obtained representative images, the spherical morphology of the particles with a mean diameter of ca. 100 nm is seen. The typical channels of the MCM-41 matrix can be easily observed as either alternate black and white stripes or a pseudohexagonal array of the pore voids in the images of solids **S1** and **S2**.

Dynamic light scattering (DLS) studies were also conducted to estimate the hydrodynamic diameter of the particles. Thus,

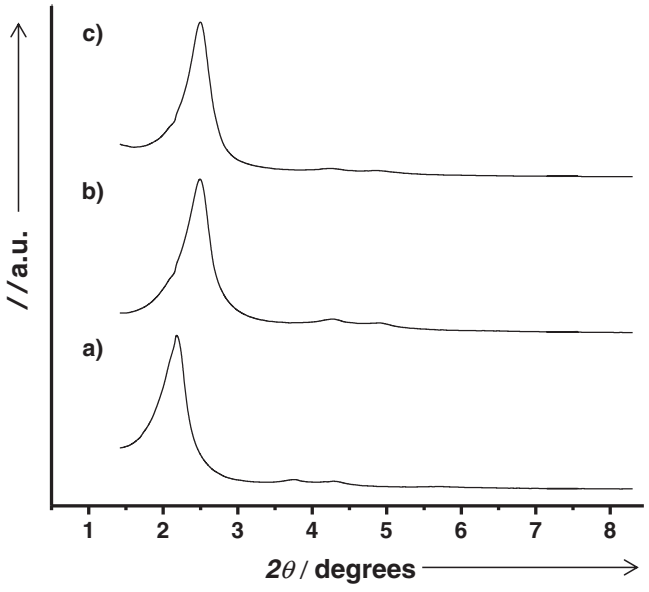

Figure 1. PXRD patterns of solids a) MCM-41 as-synthesized; b) calcined MCM-41; and c) **S1** containing the doxorubicin drug.

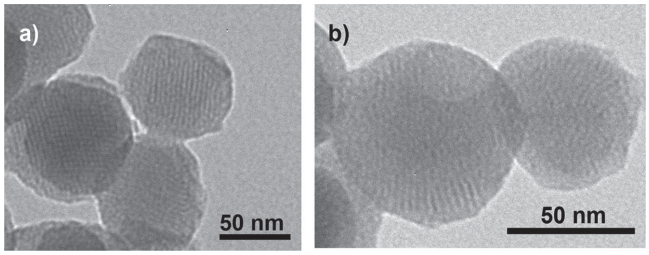

Figure 2. Representative TEM images of a) solid **S1** and b) solid **S2**.

for the calcined parent material, a narrow nanoparticle size distribution (**Figure 3**) with a mean diameter of 116 nm was obtained, while a value of 118 nm was recorded for solid **S1**.

Finally, a study of the mesopore system was conducted by recording the N_2 adsorption–desorption isotherms of the nanoparticulated calcined MCM-41 material and solid **S1**. For the calcined nanoparticles, a sharp adsorption step at an intermediate P/P_0 value (0.1–0.3) was obtained, which is typical of these solids (see **Figure 4**). Following this first step, a second adsorption process was recorded at a high relative pressure (>0.9). This adsorption profile is typical of mesoporous nanoparticles, where the first step was related to the nitrogen condensation inside the mesopores by capillarity, and the second one corresponded to the filling of the large voids among the particles, that must be considered a textural-like porosity. The application of the Brunauer-Emmett-Teller (BET) model resulted in a total specific surface value of 992.2 $m^2\ g^{-1}$ and a pore volume of 0.78 $cm^3\ g^{-1}$. The application of the Barret-Joyner-Halenda (BJH) model at the intermediate relative pressure also estimated a narrow pore distribution which centered at 2.54 nm (see the inset of Figure 4a). These data, together with the absence of a hysteresis loop in the intermediate pressure interval, suggest the existence of uniform cylindrical mesopores. By also taking into account the a_0 cell parameter calculated from PXRD (3.65 nm) and the obtained pore diameter (2.54 nm), it was possible to estimate a wall thickness value (1.11 nm).

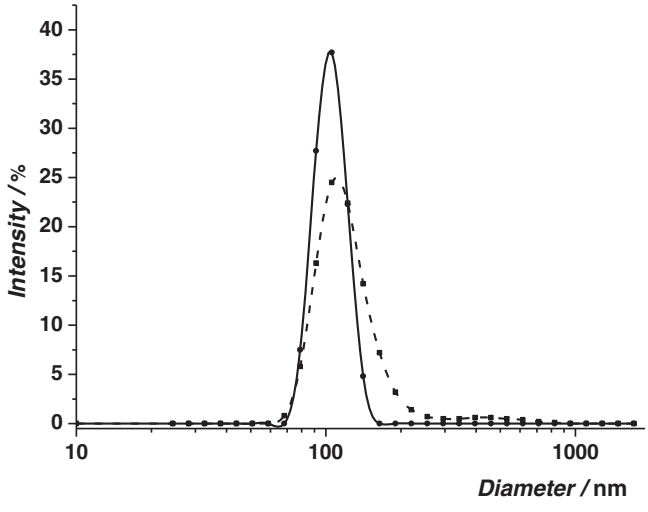

Figure 3. Size distribution by number of particles obtained in the DLS studies for calcined MCM-41 (solid line) and S1 (dashed line).

In contrast, the N_2 adsorption–desorption isotherms of **S1** recorded a sharp drop in the N_2 volume adsorbed and in the specific surface area (753.6 $m^2\ g^{-1}$) (see Figure 4). This feature is typical of mesoporous systems with at least partially filled mesopores. On the curve, apart from the adsorption step associated with the micelle-generated mesopores, a second feature also appears in the isotherm at a high relative pressure due to the textural porosity.

The BET-specific surface values, pore volumes, and pore sizes calculated from the N_2 adsorption–desorption isotherms for MCM-41 and **S1** are listed in **Table 1**.

The 1-(3-(triethoxysilyl)propyl)-3-prop-2-ynyl-urea and doxorubicin content in solid **S1** was determined by elemental and thermogravimetric analyses. In these studies, the amounts of 0.44 mmol $(gSiO_2)^{-1}$ of linker **1** and of 0.11 mmol $(gSiO_2)^{-1}$ of doxorubicin were estimated.

2.3. Doxorubicin Delivery Studies

The possibility of retaining the cargo inside a vehicle until its target is reached is a crucial, highly desirable feature in the drug delivery system to reduce side effects and increase efficiency. In this context, in vitro cargo release studies of **S2** in water, done in the presence and absence of a proteolytic enzyme obtained from *Streptomices griseus,* were performed. The prepared solid **S2** was suspended in 1 mL of water at pH 8 and then the suspension was fractionated into two parts. To one part, 4 mL of the solution containing the protease enzyme (*Streptomices griseus* enzyme; C_{enzyme} = 0.12 mg mL^{-1}, H_2O, pH 8) were added, and 4 mL of H_2O, pH 8, were added to the other part, but no enzyme was present. Both suspensions were stirred and aliquots were taken at the scheduled times. After centrifugation to eliminate the solid, the fluorescence of doxorubicin delivered to the solution was measured at 595 nm (λ_{ex} = 495 nm). The drug delivery profile in both experiments is displayed in **Figure 5**.

In the absence of the proteolytic enzyme, a remarkable flat baseline was obtained, which indicates that doxorubicin remained in the nanoparticles without release. In particular, cargo delivery was lower than 2%, even after 24 h. In contrast, a cargo release in the presence of protease was shown as an increase in doxorubicin fluorescence according to time. The observed behavior was assigned to the protease-induced hydrolysis of the peptidic bonds of the anchored peptide **P**, which resulted in the delivery of the entrapped cargo.

2.4. Evaluation of Silica Mesoporous Nanoparticles in the Toledo-B-NHL Cell Line

Controlling cell targeting and penetrability of drugs is a major issue in emerging medicine. Thus, after demonstrating the effective release of **S2**, we evaluated **S2**-induced CXCR4 internalization and its antitumor effect on Toledo B-NHL cells, which express high levels of the CXCR4 receptor in the membrane. Interaction of CXCR4 with its natural ligand, SDF-1α, has been described to induce its rapid phosphorylation and internalization.[51] In order to demonstrate the interaction of

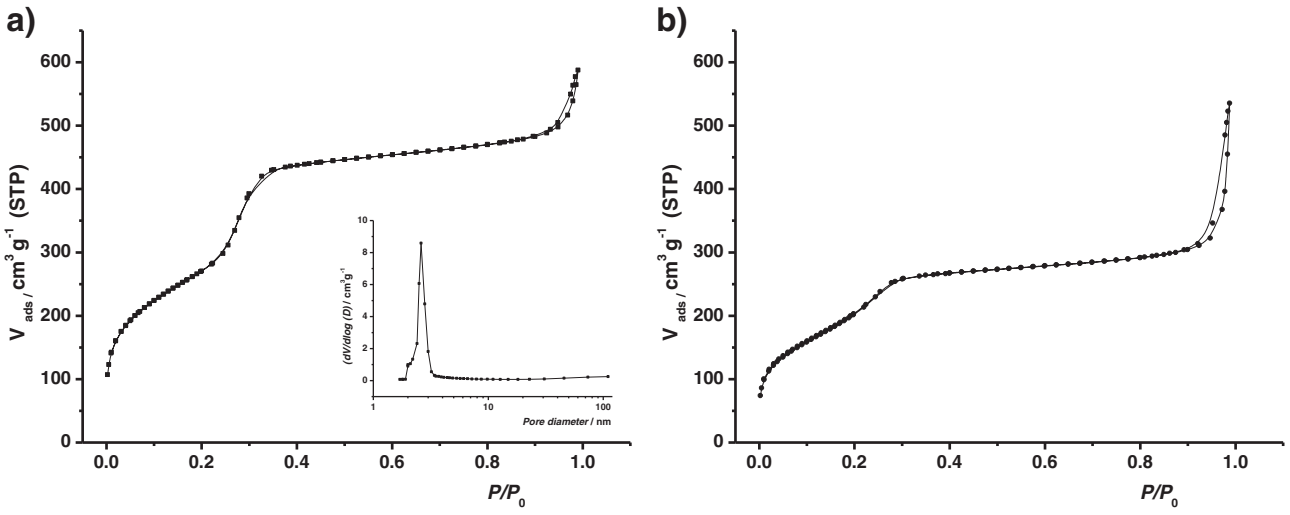

Figure 4. Nitrogen adsorption–desorption isotherms for a) MCM-41 mesoporous nanoparticles (inset: pore size distribution) and b) solid **S1**.

solid **S2** with CXCR4, followed by internalization and cargo delivery, we evaluated the effect of the nanoparticle on CXCR4 membrane levels in Toledo cells. Toledo cells were exposed to **S2** for 1 h and the CXCR4 levels in the membrane were quantified by flow cytometry. As a positive control, we also evaluated the effect of AMD3100, an antagonist of the CXCR4 receptor that triggers its internalization. Cells were also exposed to bare MSNs as a negative control. These nanoparticles contained neither doxorubicin nor gating peptide **P** and were used to see the effect of the inorganic support on the receptor expression. As shown in **Figure 6**A, Toledo cells treated with bare MSNs expressed high levels of CXCR4 in the membrane, which significantly decreased after exposure to the other tested compounds. These experiments allowed us to conclude that **S2**, like the AMD3100 antagonist, rapidly induced CXCR4 internalization, while bare MSNs did not affect the receptor expression. This evidence clearly indicates the direct interaction between the gating and targeting peptide **P** in **S2** nanoparticles and the CXCR4 chemokine receptor.

In another step, we evaluated the antitumor activity of **S2** in Toledo cells. In order to corroborate the previously observed specific CXCR4 targeting of **S2**, we also performed competition assays with the CXCR4 antagonist AMD3100. In these experiments, the viability of Toledo cells significantly decreased after exposure to **S2** (75 μg mL^{-1}) for 48 h, while cell exposure to bare MSNs had no effect on cell viability. The antitumoral effect of the **S2** nanoparticle was partially reversed when cells were preincubated with AMD3100 (see Figure 6B). Finally, apoptosis induction by **S2** was evaluated by Hoescht nuclear staining. The cells treated with the nanoparticle **S2** for 48 h showed many apoptotic bodies, which were identified by their chromatin condensation and fragmentation, as seen in Figure 6C. All these data indicated that **S2** triggers cell death in the Toledo B-NHL cells by induction of apoptosis, which is accomplished through CXCR4-dependent internalization.

The performed cellular studies indicate that **S2** selectively induces cell death in the Toledo CXCR4-expressing cells. First of all, we observed that **S2** induces CXCR4 internalization in lymphoma cells, which suggests a direct interaction between T22 peptide **P** in the nanoparticle and the chemokine receptor. Consistently, internalization of CXCR4 by the interaction with its ligand, CXCL12, has been previously described in lymphoma cells that come into contact with stromal cells,[43] and also in multiple myeloma cells.[52]

Moreover, the antitumor activity of the nanoparticle was partially reversed by the pretreatment with a CXCR4 antagonist, AMD3100, which demonstrates that its effect is, at least in part, mediated by CXCR4. The specific targeting of nanoparticles

Table 1. The BET-specific surface values, pore volumes, and pore sizes calculated from the N_2 adsorption–desorption isotherms for selected materials.

	S_{BET} [m^{2}g^{-1}]	Pore volume[a)] [cm^{3}g^{-1}]	Pore size[a,b)] [nm]	Textural pore size [nm]
MCM-41	992.2	0.78	2.54	42.00
S1	753.6	0.52	–	43.11

[a)]Pore volume and size associated with intraparticle mesopores; [b)]Pore size estimated by using the BJH model applied to the adsorption branch of the isotherm.

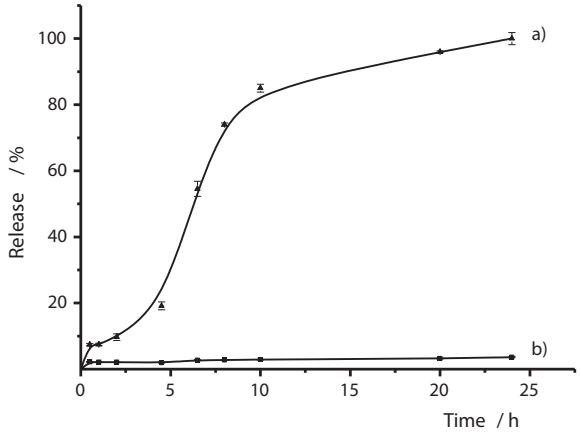

Figure 5. The release profile of S2 a) in the presence and b) absence of the enzyme.

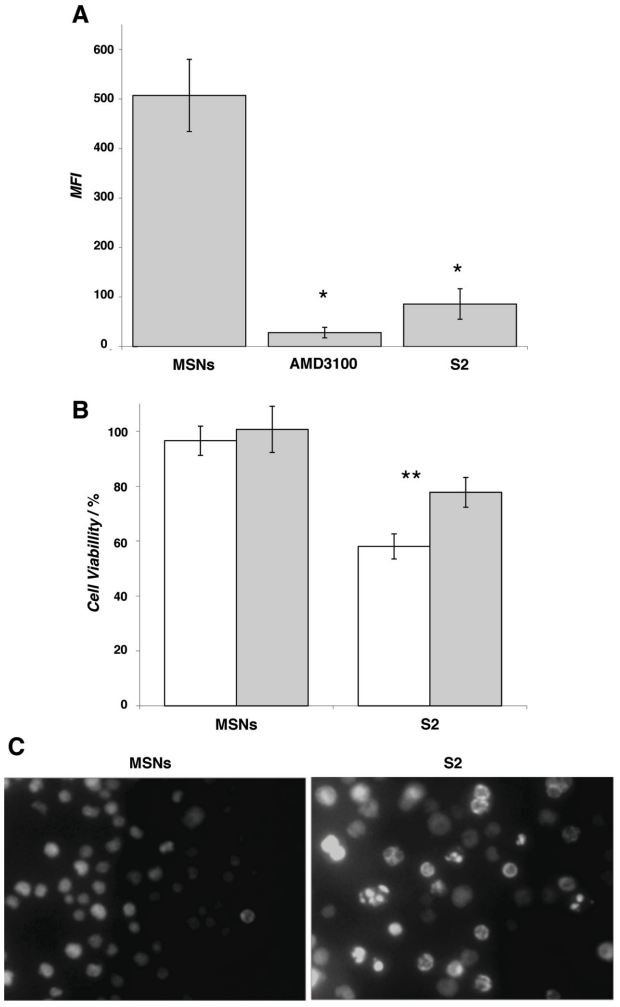

Figure 6. A) Flow cytometry analysis of the CXCR4 surface expression in Toledo cells exposed to bare MSNs (75 μg mL^{-1}), AMD3100 (10 μg mL^{-1}) and **S2** (75 μg mL^{-1}) for 1 h. B) Evaluation of cell viability inhibition by **S2** (75 μg mL^{-1}) in Toledo cells for 48 h. White bars: no pretreatment with antagonist AMD3100 (10 μg mL^{-1}). Grey bars: after a 1 h pretreatment with antagonist AMD3100 (10 μg mL^{-1}). C) Apoptosis induction after 48 h of exposure of Toledo cells to **S2** (75 μg mL^{-1}). * *P* value <0.05, ** *P* value <0.01.

to CXCR4 by the T22 ligand has previously been described in colorectal cancer cells using a protein-only nanoparticle.[49] However, this is the first time that a chemotherapeutic drug has been specifically targeted to cells expressing this receptor. CXCR4 neutralization by different molecules has been previously reported to show a strong antilymphoma effect, thus killing CXCR4-expressing lymphoma cells by a specifically designed nanosystem like **S2** can be an effective approach to reverse drug-resistance and to induce antitumor activity in B-NHL. As the CXCR4 receptor is overexpressed in other hematologic malignancies, e.g., acute myeloid leukemia, chronic lymphocytic leukemia or acute lymphoblastic leukemia,[44,45,53] in which the CXCL12/CXCR4 axis mediates cell survival and drug resistance,[54,55] the specific targeting of chemotherapeutic agents to the CXCR4 receptor could be also an effective strategy to treat different types of hematologic malignancies.

Finally, the specific targeting of doxorubicin to CXCR4-expressing cells would not only enhance its antitumor effect, but would also diminish toxicity in normal cells. Doxorubicin is an anthracycline that intercalates DNA and is commonly used to treat many types of cancers, including several hematological malignancies. However, severe adverse effects, of which cardiotoxicity is the most relevant, are frequently associated with high cumulative doses of this drug.[56] For this reason, different approaches have been developed as drug delivery systems to enhance the antitumor effect of doxorubicin, while also reducing its toxicity in normal cells. Thus, entrapment of doxorubicin into liposomes, hydrogels, and nanoparticles has been evaluated in different cancer types.[57] However, none of these formulations include the specific targeting of the drug to tumor cells. In contrast, the new delivery system **S2** proposed herein is able to conduct the delivery of a chemotherapeutic drug to CXCR4-expressing cells. Specificity of delivery would enhance the antitumor effect in tumor cells, which overexpress CXCR4, and would diminish toxicity in normal cells.

4. Conclusion

In summary, we have developed a CXCR4-targeted delivery system using MSN containing T22 analogue peptide **P** as a dual functional element. In the prepared nanosystem, peptide **P** was able to cap the pores in MSN to block the release of the doxorubicin drug. Anchored peptide **P** also guides the capped nanoparticle to B-NHL cells and facilitates MSN uptake via the CXCR4 receptor. The endocyted capped MSN were opened thanks to the proteolytic enzymes present in the lysosomes, which degrade peptide **P** and allow doxorubicin delivery. These can be considered a preliminary result towards adopting new therapeutic strategies to kill CXCR4-expressing lymphoma cells. This is also one of the few examples that use peptides as a targeting and capping element in MSNs. We believe that the synthetic strategy followed herein, which combines the use of mesoporous nanoparticles with highly specific targeting peptides, can contribute to further design improved delivery systems for other specific diseases.

5. Experimental Section

Chemicals: The chemicals tetraethyl orthosilicate (TEOS), *n*-cetyltrimethylammonium bromide (CTABr), sodium hydroxide (NaOH), protease from *Streptomyces griseus,* fluorescein, and CXCR4 inhibitor AMD3100 were acquired from Sigma-Aldrich and were used without further purification. Copper (II) sulphate pentahydrate ($CuSO_4{\cdot}5H_2O$) and sodium ascorbate were purchased from Scharlab. Doxorubicin hydrochloride was obtained from Sequoia. The H-Rink amide ChemMatrix resin was provided by PCAS BioMatrix Quebec, Canada. Solvents MeOH, DMF, DCM, tert-butylmethyl ether, ACN, DMSO and the reactives TFA, DIEA, HBTU, piperidine, DIPCDI, HOAt, TIS were supplied by Sigma-Aldrich, Carlo Erba SDS, and Panreac. The amino acid C-terminal, Fmoc-Arg(Pbf)-OH, was purchased from Iris Biotech.

General Techniques: The T22 peptide analogue was synthesized using instrumentation in the CIBER BBN Synthesis of Peptide Unit. UV spectroscopy, HPLC, and HPLC-MS were used for the analysis and purification of the azide-containing T22 peptide. UV measurements were taken on a UV–vis Recording Spectrophotometer UV-2501PC at 290 nm. Analytical reversed phase HPLC (RP-HPLC) was carried out in a

Waters instrument comprising a XBridge™ BEH130 C18 reversed-phase HPLC analytical column (4.6 × 100 mm, 3.5 µm; Waters), a separation module (Waters 2695), an automatic injector (Waters 717 autosampler), and a photodiode array detector (Waters 2298). Data were processed with the Empower 2 software. UV detection was performed at 220 nm, and the linear gradients from 5%B to 100%B were run at a flow rate of 1.0 mL min^{-1} for 8 min. The elution solvent system was: A: H_2O (+0.045% TFA) and B: ACN (+0.036% TFA). The HPLC-MS analyses of peptide samples were carried out in a Waters instrument comprising a Sunfire™ C18 reversed-phase analytical column (2.1 × 100 mm, 5 µm; Waters), a separation module (Waters 2695), an automatic injector (Water 717 autosampler), a photodiode array detector (Waters 2298), and a Waters micromass ZQ spectrometer unit. Data were processed with the MassLynx V4.1 software (Waters). UV detection was performed at 220 nm, and the linear gradients of ACN (+0.07% formic acid) in H_2O (+0.1% formic acid) were run at a flow rate of 0.3 mL min^{-1} for 8 min. HPLC purification was carried out by semipreparative RP-HPLC in a Waters instrument comprising a Sunfire™ C18 reversed-phase semipreparative column, 5.0 µm, 19 × 100 mm, a separation module (Waters Delta 600), a Waters 600 controller, an automatic injector (Waters 2700), a dual absorbance detector (Waters 2487) and a fraction collector II (Waters). UV detection was performed at 220 nm, and the linear gradients from 5%B to 100%B were run at a flow rate of 15.0 mL min^{-1} over 20 min. The elution solvent system was: A:H_2O (+0.1% TFA) and B: CH_3CN (+0.05% TFA). Powder X-ray diffraction (PXRD), thermogravimetric analysis (TGA), elemental analysis, transmission electron microscopy TEM) and N_2 adsorption–desorption were employed to characterize the prepared materials. PXRD measurements were taken with a Philips D8 Advance diffractometer using CuKα radiation. The TGA analyses were carried out on a TGA/SDTA 851e Mettler Toledo balance using an oxidant atmosphere (air, 80 mL min^{-1}) with a heating program consisting in a heating ramp of 10 °C per minute from 393 to 1273 K, and an isothermal heating step at this temperature lasting 30 min. Fluorescence spectroscopy was carried out on a JASCO FP-8300 fluorimeter. TEM images were obtained with a 100 kV Philips CM10 microscope.

Synthesis of the Propargyl-Containing Linker **1**: 1.28 mL (5 mmol) of 3-(triethoxysilyl)propylisocyanate with 320 µL (5 mmol) of propargylamine were reacted in 15 mL of CH_2Cl_2 overnight. Then the solvent was evaporated to obtain the final propargyl-containing product 1-(3-(triethoxysilyl)propyl)-3-prop-2-ynyl-urea (**1**), as depicted in Scheme SI-1, Supporting Information. The obtained product was characterized by ^{1}H NMR (400 MHz, $CDCl_3$): δ 0.53 (t, 2H), 1.11 (t, 3H), 1.50 (qt,2H), 2.12 (t, 1H), 3.06 (qd, 2H), 3.70 (qd, 2H), 3.85 (qd,2H), 5.85(dt, 1H) ppm; ^{13}C NMR (101 MHz, $CDCl_3$) δ 158.40, 80.91, 70.24, 57.58, 42.53, 29.36, 23.22, 17.72, 7.32; HRMS-EI *m/z*: calcd for $C_{13}H_{26}N_2O_4Si$ 302.1662; found: 302.1683; FT-IR typical urea bands were found (see Supporting Information for more details).

Solid-Phase Synthesis of the T22 Analogue ([Tyr^{5,12}Lys^7]Polyphemusin II)1: An azide-containing analogue of T22 (**P**) with Lys(N_3) in the N-Terminal was obtained using all the Cys side chains protected with Trt. For this purpose, 200 mg of the H-Rink amide ChemMatrix resin (0.114 mmol; loading 0.57 mmol g^{-1}) were washed with MeOH, DMF, DCM and TFA/DCM 1%, DMF, DCM and DIEA 5%/DCM, DMF and DCM. The amino acid C-terminal Fmoc-Arg(Pbf)-OH (0.220 mg; 0.3 mmol) was introduced into the resin using as a coupling system HBTU (0.130 mg; 0.3 mmol) and DIEA (0.078 mL; 0.4 mmol) in DMF, and the mixture was shaken for 1 h. Then the Fmoc-Arg(Pbf)-Rink amide resin was filtered and washed with DMF (5 × 1 min) and DCM (5 × 1 min). The Fmoc group was eliminated by treatments with piperidine-DMF (1:4; 25 mL g^{-1} resin; 2 × 5 min). Filtrates were collected and quantified by UV (290 nm) to obtain a loading of 0.50 mmol g^{-1}. Based on this loading, the following protected amino acids were incorporated (3 equiv each) using HBTU (3 equiv) and DIEA (4 equiv) into the DMF as coupling system with 60-s preactivation, except for Fmoc-Cys(Trt)-OH (3 equiv). This was incorporated using DIPCDI (3 equiv) and HOAt (3 equiv) into DMF by a 3-min preactivation to avoid epimerization. Washes between couplings and the Fmoc group elimination steps were performed using DMF (5 × 1 min) and DCM (5 × 1 min). Having finished peptide elongation, the peptide was cleaved from the resin using the mixture TFA-TIS-H_2O (95:2.5:2.5, 30 mL) at 25 °C for 1 h. F were separated by filtration from the resin and were partially evaporated and then precipitated by addition of cold tert-butylmethyl ether. The suspension was centrifuged, the supernatant was discarded, and the solid was dissolved in H_2O-ACN (1:1) and lyophilized to obtain 250 mg of the linear peptide crude depicted in Scheme SI-2, Supporting Information (yield: 83%; purity: 85%).

T22 Analogue Cyclization ([Tyr^{5,12}Lys^7]Polyphemusin II): The obtained peptide was oxidized for its cyclization. To this end, the linear peptide precursor (100 mg, 3.78 × 10^{-5} mol) was dissolved in water-acetonitrile (1:1; 126 mL, 3 × 10^{-4} M) and pH was adjusted to 8 with aqueous ammonia. DMSO was added (5% of the total volume) as the oxidizing agent. The reaction was stirred for 12 h at room temperature and monitored by HPLC. After reaction completion, the solvent was removed by lyophilization to obtain 96 mg of the cyclic peptide crude (yield: 96%). The crude was purified by semipreparative HPLC-MS (Figure SI-2, Supporting Information) and fractions were collected to obtain the final azide-T22 analogue (**P**), which is seen in Scheme S2, Supporting Information.

Synthesis of Mesoporous Silica Nanoparticles: MCM-41 mesoporous nanoparticles were synthesized by the following procedure: *n*-cetyltrimethylammonium bromide (CTABr, 1.00 g, 2.74 mmol) was first dissolved in 480 mL of deionized water. Then 3.5 mL of NaOH 2.00 M in deionized water were added to the CTABr solution, and then the solution temperature was adjusted to 80 °C. At that time, TEOS (5.00 mL, 2.57 × 10^{-2} mol) was added dropwise to the surfactant solution. The mixture was allowed to stir for 2 h to give a white precipitate. After this time, the solid product was centrifuged, washed with deionized water and ethanol, and dried at 60 °C to give MCM-41 as-synthesized mesostructured nanoparticles. To obtain the final porous nanoparticulated material (MSNs), the as-synthesized solid was calcined at 550 °C in an oxidant atmosphere for 5 h to remove the template phase.

*Synthesis of Solid **S1***: MSNs solid support (190 mg) and doxorubicin hydrochloride (96 mg, 0.17 mmol) were suspended in Milli-Q water (7.5 mL) and stirred for 24 h at room temperature to achieve maximum loading in the pores of the MCM-41-type scaffolding. Then the solid was filtered and dried under vacuum. In another step, 192 mg of the doxorubicin loaded solid were suspended in 30 mL of acetonitrile and 0.96 mmol of the propargyl-containing linker **1** were added. The mixture was stirred for 5.5 h, then filtered, washed with acetonitrile, and dried under vacuum to yield red-pink solid **S1**.

*Synthesis of Solid **S2***: To prepare solid **S2**, previously functionalized nanoparticles **S1** (12 mg) and azide-containing T22 peptide **P** (15 mg) were suspended in a 50:50 v/v DMF-H_2O mixture (10 mL) in the presence of excess doxorubicin (5 mg, 0.008 mmol) to avoid the delivery of the drug from pores to the bulk solution during synthesis. Then 5.7 µL of a solution of $CuSO_4{\cdot}5H_2O$ (10^{-3} mol L^{-1}) and 5.7 µL of sodium ascorbate (10^{-2} mol L^{-1}) were added. The reaction mixture was stirred at room temperature for 3 d. Then the nanoparticles were centrifuged and washed thoroughly with water to remove unreacted and absorbed molecules. The resulting red-pink nanoparticles were dried under vacuum to yield capped solid **S2**. This solid contained doxorubicin in the pore voids and the T22 analogue peptide **P** was anchored in the pore outlets, as depicted in Scheme SI-3, Supporting Information.

Cell Lines and Culture Conditions: Toledo is a human nonHodgkin's lymphoma cell line obtained from the American Type Culture Collection. Toledo cells were cultured with RPMI 1640 supplemented with 10% fetal bovine serum, 1% glutamine, 100 U mL^{-1} penicillin/streptomycin (Life Technologies) and incubated at 37 °C in a humidified atmosphere containing 5% CO_2.

FACS Analysis: A fluorescence-activated cell sorting (FACS) analysis was performed to evaluate CXCR4 membrane expression in the Toledo cells exposed to calcined MCM-41 nanoparticles, solid **S2** (75 µg mL^{-1}) or AMD3100 (10 µg mL^{-1}) for 1 h. For each sample, 3 × 10^6 cells were washed in phosphate-buffered saline (PBS) and incubated for 30 min

at 4 °C with the PE-Cy5 mouse antihuman CXCR4 monoclonal antibody or PE-Cy5 mouse IgG2a (BD Pharmingen) as an isotype control. Cells were washed twice with PBS and the cell surface expression of CXCR4 was detected by flow cytometry (FACS Calibur, BD). Data were analyzed with the Cell Quest Pro software. The results are expressed as the mean fluorescence intensity (MFI) ± SD.

Cytotoxicity Assays: The antitumor activity of solid **S2** was evaluated by measuring cell metabolic capacity (viability) using the Cell Proliferation Kit II (XTT) (Roche Diagnostics) and following the manufacturer's recommendations. Briefly, Toledo cells were seeded into 96-well plates (30×10^4 cells/well) and exposed to calcined MCM-41 nanoparticles (PBS) or solid **S2** (75 μg mL^{-1}), with or without a 1 h pretreatment with AMD3100. After a 48-h exposure at 37 °C, XTT detection solution was added to the wells and absorbance was measured at the 450 nm wavelength with a spectrophotometer. Growth inhibitory activity was expressed as a percentage of cell viability, as compared with the untreated controls. Values are the averages of the replicates performed in at least two independent experiments.

Apoptotic Detection and DNA Fragmentation: To evaluate the induction of apoptosis, nuclear staining was performed with Hoescht 3342 dye (Sigma) in the cells exposed to calcined MCM-41 nanoparticles (PBS) or solid **S2** (75 μg mL^{-1}) for 48 h. During exposure, 2 μL mL^{-1} of Hoescht dye were added to the cell culture and live cells were observed under a fluorescence microscope (Zeiss).

Statistical Analysis: The cell viability or MFI data were compared with the Mann–Whitney *U*-test. Differences at $p < 0.05$ were considered statistically significant. A statistical analysis was performed using the SPSS Software (SPSS Statistics 21).

Supporting Information

Supporting Information is available from the Wiley Online Library or from the author.

Acknowledgements

Financial support from the Spanish Government (MAT2012–38429-C04 and PIB2010BZ-00563), Generalitat Valenciana (PROMETEOII/2014/047), Generalitat de Catalunya (2009-SGR-1437), Instituto de Salud Carlos III (FI10/00758 and FIS PII2/01861), MaratóTV3 416/C/2013–2030, CIBER-BBN (Nanomets), and Institut de Recerca Josep Carreras Sant Pau is gratefully acknowledged. C.T. is grateful to the Spanish MEC for her grant. The authors also acknowledge Cristina Suárez for her technical support and the use of the CIBER-BBN Nanotoxicology and Synthesis of Peptides platforms.

Received: October 30, 2014
Published online: December 17, 2014

[1] a) M. Vallet-Regí, F. Balas, D. Arcos, *Angew. Chem.* **2007**, *119*, 7692; b) M. Vallet-Regí, F. Balas, D. Arcos, *Angew. Chem Int. Ed.* **2007**, *46*, 7548.
[2] K. M. L. Taylor-Pashow, J. Della Rocca, R. C. Huxford, W. Lin, *Chem. Commun.* **2010**, *46*, 5832.
[3] a) P. Yang, S. Gai, J. Lin, *Chem. Soc. Rev.* **2012**, *41*, 3679; b) Z. Li, J. Barnes, A. Bosoy, J. F. Stoddart, J. I. Zink, *Chem. Soc. Rev.* **2012**, *41*, 2590.
[4] M. Colilla, B. González, M. Vallet-Regí, *Biomater. Sci.* **2013**, *1*, 114.
[5] Q. He, J. Shi, *J. Mater. Chem.* **2011**, *21*, 5845.
[6] C.-Y Lai, B. G. Trewyn, D. M. Jeftinija, K. Jeftinija, S. Xu, S. Jeftinija, V. S.-Y. Lin, *J. Am. Chem. Soc.* **2003**, *125*, 4451.
[7] C. Park, K. Oh, S. C. Lee, C. Kim, *Angew. Chem Int. Ed.* **2007**, *46*, 1455.
[8] R. Liu, X. Zhao, T. Wu, P. Feng, *J. Am. Chem. Soc.* **2008**, *130*, 14418.
[9] a) Z. Luo, K. Cai, Y. Hu, L. Zhao, P. Liu, L. Duan, W. Yang, *Angew. Chem.* **2011**, *123*, 666; b) Z. Luo, K. Cai, Y. Hu, L. Zhao, P. Liu, L. Duan, W. Yang, *Angew. Chem Int. Ed.* **2011**, *50*, 640.
[10] a) C. Wang, Z. Li, D. Cao, Y.-L. Zhao, J. W. Gaines, O. A. Bozdemir, M. W. Ambrogio, M. Frasconi, Y. Y. Botros, J. I. Zink, J. F. Stoddart, *Angew. Chem.* **2012**, *124*, 5556; b) C. Wang, Z. Li, D. Cao, Y.-L. Zhao, J. W. Gaines, O. A. Bozdemir, M. W. Ambrogio, M. Frasconi, Y. Y. Botros, J. I. Zink, J. F. Stoddart, *Angew. Chem Int. Ed.* **2012**, *51*, 5460.
[11] Y. Zhang, Q. Yuan, T. Chen, X. Zhang, Y. Chen, W. Tan, *Anal. Chem.* **2012**, *84*, 1956.
[12] D. Tarn, M. Xue, J. I. Zink, *Inorg. Chem.* **2013**, *52*, 2044.
[13] N. K. Mal, M. Fujiwara, Y. Tanaka, *Nature* **2003**, *421*, 350.
[14] a) A. Schlossbauer, S. Warncke, P. M. E. Gramlich, J. Kecht, A. Manetto, T. Carell, T. Bein, *Angew. Chem.* **2010**, *122*, 4842; b) A. Schlossbauer, S. Warncke, P. M. E. Gramlich, J. Kecht, A. Manetto, T. Carell, T. Bein, *Angew. Chem Int. Ed.* **2010**, *49*, 4734.
[15] E. Ruiz-Hernández, A. Baeza, M. Vallet-Regi, *ACS Nano* **2011**, *5*, 1259.
[16] D. He, X. He, K. Wang, J. Cao, Y. Zhao, *Adv. Funct. Mater.* **2012**, *22*, 4704.
[17] E. Aznar, L. Mondragón, J. V. Ros-Lis, F. Sancenón, M. D. Marcos, R. Martínez-Máñez, J. Soto, E. Pérez-Payá, P. Amorós, *Angew. Chem Int. Ed.* **2011**, *50*, 11172.
[18] A. Baeza, E. Guisasola, E. Ruiz-Hernández, M. Vallet-Regi, *Chem. Mater.* **2012**, *24*, 517.
[19] a) A. Schlossbauer, J. Kecht, T. Bein, *Angew. Chem.* **2009**, *121*, 3138; b) A. Schlossbauer, J. Kecht, T. Bein, *Angew. Chem Int. Ed.* **2009**, *48*, 3092.
[20] C. Park, H. Kim, S. Kim, C. Kim, *J. Am. Chem. Soc.* **2009**, *131*, 16614.
[21] A. Bernardos, L. Mondragón, E. Aznar, M. D. Marcos, R. Martínez-Máñez, F. Sancenón, J. Soto, J. M. Barat, E. Pérez-Payá, C. Guillem, P. Amorós, *ACS Nano* **2010**, *4*, 6353.
[22] P. D. Thornton, A. Heise, *J. Am. Chem. Soc.* **2010**, *132*, 2024.
[23] a) A. Popat, B. P. Ross, J. Liu, S. Jambhrunkar, F. Kleitz, S. Z. Qiao, *Angew. Chem.* **2012**, *124*, 12654; b) A. Popat, B. P. Ross, J. Liu, S. Jambhrunkar, F. Kleitz, S. Z. Qiao, *Angew. Chem Int. Ed.* **2012**, *51*, 12486.
[24] Z. Chen, Z. Li, Y. Lin, M. Yin, J. Ren, X. Qu, *Chem. Eur. J.* **2013**, *19*, 1778.
[25] C. E. Ashley, E. C. Carnes, G. K. Phillips, D. Padilla, P. N. Durfee, P. A. Brown, T. N. Hanna, J. Liu, B. Phillips, M. B. Carter, N. J. Carroll, X. Jiang, D. R. Dunphy, C. L Willman, D. N. Petsev, D. G. Evans, A. N. Parikh, B. Chackerian, W. Wharton, D. S. Peabody, *Nat. Mater.* **2011**, *10*, 389.
[26] a) C. Coll, L. Mondragón, R. Martínez-Mañez, F. Sancenón, M. D. Marcos, J. Soto, P. Amorós, E. Pérez-Payá, *Angew. Chem.* **2011**, *123*, 2186; b) C. Coll, L. Mondragón, R. Martínez-Mañez, F. Sancenón, M. D. Marcos, J. Soto, P. Amorós, E. Pérez-Payá, *Angew. Chem Int. Ed.* **2011**, *50*, 2138.
[27] K. Radhakrishnan, S. Gupta, D. Gnanadhas, P. C. Ramamurthy, D. Chakravortty, A. M. Raichur, *Part. Part. Syst. Charact.* **2014**, *31*, 449.
[28] C. de la Torre C, A. Agostini, L. Mondragón, M. Orzáez, F. Sancenón, R. Martínez-Máñez, M. D. Marcos, P. Amorós, E. Pérez-Payá, *Chem Commun.* **2014**, *50*, 3184.
[29] L. Mondragón, N. Mas, V. Ferragud, C. de la Torre, A. Agostini, R. Martínez-Máñez, F. Sancenón, P. Amorós, E. Pérez-Payá, M. Orzáez, *Chem. Eur. J.* **2014**, *20*, 5271.
[30] J. Zhenga, X. Tiana, Y. Sunb, D. Lub, W. Yanga, *Int. J. Pharmaceutics* **2013**, *450*, 296.
[31] K. Murai, M. Higuchi, T. Kinoshita, K. Nagataa, K. Kato, *Phys. Chem. Chem. Phys.* **2013**, *15*, 11454.

[32] D. M. Copolovici, K. Langel, E. Eriste, U. lo Langel, *ACS Nano* **2014**, *8*, 1972.
[33] Q. Zhang, X. Wang, P.-Z. Li, K. T. Nguyen, X.-J. Wang, Z. Luo, H. Zhang, N. S. Tan, Y. Zhao, *Adv. Funct. Mater.* **2014**, *24*, 2450.
[34] C. E. Ashley, E. C. Carnes, K. E. Epler, D. P. Padilla, G. K. Phillips, R. E. Castillo, D. C. Wilkinson, B. S. Wilkinson, C. A. Burgard, R. M. Kalinich, J. L. Townson, B. Chackerian, C. L. Willman, D. S. Peabody, W. Wharton, C. J. Brinker, *ACS Nano* **2012**, *6*, 2174.
[35] Q. Zhang, F. Liu, K. T. Nguyen, X. Ma, X. Wang, B. Xing, Y. Zhao, *Adv. Funct. Mater.* **2012**, *22*, 5144.
[36] Z. Luo, K. Cai, Y. Hu, L. Zhao, P. Liu, L. Duan, W. Yang, *Angew. Chem Int. Ed.* **2011**, *50*, 640.
[37] J. Zhang, Z.-F. Yuan, Y. Wang, W.-H. Chen, G.-F. Luo, S.-X. Cheng, R.-X. Zhuo, X.-Z. Zhang, *J. Am. Chem. Soc.* **2013**, *135*, 5068.
[38] Z. Zhao, H. Meng, N. Wang, M. J. Donovan, T. Fu, M. You, Z. Chen, X. Zhang, W. Tan, *Angew. Chem Int. Ed.* **2013**, *52*, 7487.
[39] P. Feugier, A. Van Hoof, C. Sebban, P. Solal-Celigny, R. Bouabdallah, C. Fermé, B. Christian, E. Lepage, H. Tilly, F. Morschhauser, P. Gaulard, G. Salles, A. Bosly, C. Gisselbrecht, F. Reyes, B. Coiffier, *J. Clin. Oncol.* **2005**, *23*, 4117.
[40] M. Pfreundschuh, E. Kuhnt, L. Trümper, A. Österborg, M. Trneny, L. Shepherd, D. S. Gill, J. Walewski, R. Pettengell, U. Jaeger, P.-L. Zinzani, O. Shpilberg, S. Kvaloy, P. N. Brown, R. Stahel, N. Milpied, A. López-Guillermo, V. Poeschel, S. Grass, M Loeffler, N. Murawski, *Lancet Oncol.* **2011**, *12*, 1013.
[41] S. Cultrera, S. Dalia, *Cancer Control* **2012**, *19*, 204.
[42] J. Linderoth J, P. Edén, M. Ehinger, J. Valcich, M. Jerkeman, O. Bendahl, M. Berglund, G. Enblad, M. Erlanson, G. Roos, E. Cavallin-Ståhl, *Br. J. Haematol.* **2008**, *141*, 423.
[43] J. Arai, M. Yasukawa, Y. Yakushijin, T. Miyazaki, S. Fujita, *Eur. J. Haematol.* **2000**, *64*, 323.
[44] N. Ishibe, M. Albitar, I. Jilani, L. R. Goldin, G. E. Marti, N. E. Caporaso, *Blood* **2002**, *100*, 1100.
[45] S.-Y. Ko, C.-J. Park, S.-H. Park, Y.-U. Cho, S. Jang, E.-J. Seo, N. Kim, D.-Y. Kim, K. N. Koh, H. J. Im, J.-J. Seo, H.-S. Chi, *Leuk. Res.* **2014**, *38*, 65.
[46] M. J. Moreno, R. Dieguez-Gonzalez, S. Novelli, A. Mozos, A. Gallardo, M. A. Pavón, M. V. Céspedes, A. Grañena, M. Alcoceba, O. Blanco, M. Gonzalez-Díaz, J. Sierra, R. Mangues, I. Casanova, *J. Pathol.* **2014**, DOI: 10.1002/path.4446.
[47] X. Liang, *Chem. Biol. Drug Des.* **2008**, *72*, 97.
[48] T. Murakami, T.-Y. Zhang, Y. Koyanagi, Y. Tanaka, J. Kim, Y. Suzuki, S. Minoguchi, H. Tamamura, M. Waki, A. Matsumoto, N. Fujii, H. Shida, J. A. Hoxie, S. C. Peiper, N. Yamamoto, *J. Virol.* **1999**, *73*, 7489.
[49] U. Unzueta, M. V. Céspedes, N. Ferrer-Miralles, I. Casanova, J. Cedano, J. L. Corchero, J. Domingo-Espín, A. Villaverde, R. Mangues, E. Vázquez, *Int. J. Nanomed.* **2012**, *7*, 4533.
[50] H. Tamamura, M. Imai, T. Ishihara, M. Masuda, H. Funakoshi, H. Oyake, T. Murakami, R. Arakaki, H. Nakashima, A. Otaka, T. Ibuka, M. Waki, A. Matsumoto, N. Yamamoto, N. Fujii, *Bioorg. Med. Chem.* **1998**, *6*, 1033.
[51] J. M. Busillo, J. L. Benovic, *Biochim. Biophys. Acta* **2007**, *1768*, 952.
[52] Y. Alsayed, H. Ngo, J. Runnels, X. Leleu, U. K. Singha, C. M. Pitsillides, J. A. Spencer, T. Kimlinger, J. M. Ghobrial, X. Jia, G. Lu, M. Timm, A. Kumar, D. Côté, I Veilleux, K. E. Hedin, G. D. Roodman, T. E. Witzig, A. L. Kung, T. Hideshima, K. C. Anderson, C. P. Lin, I. M. Ghobrial, *Blood* **2007**, *109*, 2708.
[53] A. C. Spoo, M. Lübbert, W. G. Wierda, J. A. Burger, *Blood* **2007**, *109*, 786.
[54] M. B. Meads, L. A. Hazlehurst, W. S. Dalton, *Clin. Cancer Res.* **2008**, *14*, 2519.
[55] S. López-Giral, N. E. Quintana, M. Cabrerizo, M. Alfonso-Pérez, M. Sala-Valdés, V. G. De Soria, J. M. Fernández-Rañada, E. Fernández-Ruiz, C. Muñoz, *J. Leukoc. Biol.* **2004**, *76*, 462.
[56] Y. Shi, M. Moon, S. Dawood, B. McManus, P. P. Liu, *Herz* **2011**, *36*, 296.
[57] O. Tacar, P. Sriamornsak, C. R. Dass, *J. Pharm. Pharmacol.* **2013**, *65*, 157.